Desalination and Water Treatment
www.deswater.com

doi:10.5004/dwt.2019.24638

166 (2019) 92–104
October

A brief study on the boosted photocatalytic activity of AgI/WO_3/ZnO in the degradation of Methylene Blue under visible light irradiation

Shirin Ghattavi[a,b,c], Alireza Nezamzadeh-Ejhieh[a,b,d,*]

[a]*Department of Chemistry, Shahreza Branch, Islamic Azad University, P.O. Box 311-86145, Shahreza, Isfahan, Iran,*
[b]*Young Researchers and Elite Club, Shahreza Branch, Islamic Azad University, Shahreza, Iran*
[c]*Department of Chemistry, Firoozabad Branch, Islamic Azad University, Firoozabad, Iran, email: ghattavi_44@yahoo.com (S. Ghattavi)*
[d]*Razi Chemistry Research Center (RCRC), Shahreza Branch, Islamic Azad University, Isfahan, Iran,*
email: arnezamzadeh@iaush.ac.ir (A. Nezamzadeh-Ejhieh)

Received 25 February 2019; Accepted 29 June 2019

ABSTRACT

A novel visible-light-driven AgI/WO_3/ZnO nanocomposite was synthesized for the photodegradation of methylene blue (MB). The composite was characterized by XRD, UV-Vis DRS, SEM, BET, electrochemical impedance spectroscopy (EIS) and photoluminescence (PL) techniques. PL results confirmed lower PL intensity for the composite confirming a lower e^-/h^+ recombination for it. Both PL intensity and photodegradation activity of the resulted composites depended on the mole ratio of AgI, WO_3 and ZnO in the composite. The composite with a mole ratio of 2:1:1 (AgI:WO_3:ZnO) showed a broad PL peak at 698 nm which is 11.3 times weaker than that of WO_3 and ZnO and 3 times weaker than that of AgI alone. Among the composites with different mole ratios, this composite had also the lowest PL intensity. Initial photodegradation experiments showed that about 21%, 36%, 56% and 69% of MB molecules can remove by single ZnO, WO_3, AgINps and the composite (with a mole ratio of 1:1:1), respectively. The composite with a mole ratio of 2:1:1 showed also the best photodegradation efficiency and it removed about 79% of MB molecules during 40 min photodegradation process. MB solutions before and after photodegradation process were subjected to FTIR analysis and the results showed appearance of new peaks at 3452 and 1655 cm^{-1}, confirming degradation of MB molecules into the smaller fragments. The pseudo-first order reaction rate constants of 0.055 and 0.025 min^{-1} were estimated based on COD and UV-Vis results based on the Hinshelwood model. The catalyst showed good reusing applicability after 4 successive runs.

Keywords: AgI; WO_3; ZnO; Methylene Blue; Photodegradation catalysis; Composite

1. Introduction

Nowadays, due to climate change and poor management for water resource, the implementation of water reclamation and reuse is gotten an increased attention. In general, increased need for clean water is a vital need of body life. This is a major global problem with expanding global economy and population countries [1,2]. Hence, removal of pollutants from water/wastewater is a prime importance in health/environmental point of views [3,4]. Traditional methods (precipitation, flotation, adsorption etc.) can only concentrate or change the organic/inorganic pollutants from aqueous phase to a solid phase. Thus, additional cost need for the treatment of the secondary pollutants and regeneration of the used adsorbent [5]. Hence, advanced oxidation processes (AOPs) based on in situ generation of strong chemical oxidants (for example, OH and superoxide radicals) with the assistance of O_3, H_2O_2, Fenton's reagent, UV irradiation or a catalyst have been widely used for the removing of different pollutants, especially for the low biodegradability pollutants, from water/wastewater samples [6,7]. Generally, advantages of AOPs are: (i) fast degradation speed, (ii) ability to mineralize the organic pollutants to green compounds, (iii) ability to act at ambient

*Corresponding author.

conditions, and (iv) decrease the toxicity of organic pollutants [8]. The most common AOP technique is the heterogeneous semiconducting based photocatalysis in which the photogenerated electron-hole (e^-/h^+) pairs on the valence (V_b) and conduction (C_b) bands of the illuminated semiconductor can react with dissolved oxygen or water/hydroxyl to form super oxide and hydroxyl radicals, respectively. All e^-/h^+ pairs and the aforementioned radicals are reactive species that can destroy different organic pollutants in water non-selectively, and finally mineralize them to CO_2 and watermolecules [9–17]. Unfortunately, recombination of e^-/h^+ pairs in this technique significantly reduces its photocatalytic ability. So far, different alternatives of doping, coupling of semiconductors, using nano-dimension, supporting of semiconductors have been used for increasing the photocatalytic activity of single semiconductor systems. In nano-dimension approach, the generated e^-/h^+ pairs can rapidly immigrate to the catalyst surface, due to the decreased path-length, before they can recombine with together [18–23].

In the present work, ZnO, AgI and WO_3 were coupled and the resulted composite was used in the photodegradation of methylene blue (MB) in aqueous solution. ZnO is an excellent semiconductor oxide (band gap width: 3.37 eV, excitation binding energy: 60 meV) with ultraviolet (UV) absorption ability, possesses the excellent electrical, mechanical, optical and antifouling and antibacterial properties, comparable with TiO_2. It is a cost effective catalyst with respect to TiO_2 and Al_2O_3. Fast e^-/h^+ recombination of ZnO and its large absorption edge in UV region of solar light have limited its photocatalytic application. Accordingly, enhance in its optical band gap (minimizing) for absorbing solar light and inhibiting the e^-/h^+ recombination are interesting subject for researchers [17,24–29].

WO_3 with ability to absorb the blue region of the solar light, (band gap energy: 2.4–2.8 eV) has a much positive valence band edge (3.4 eV) than the H_2O/O_2 oxidation potential that is suitable for photo-oxidation of organic pollutants. Nevertheless, its more positive conduction band level (0.74 eV vs NHE) than the potential of the oxygen reduction, caused to a fast e^-/h^+ recombination process. This has been overcame by loading Pt and solid state ionics such as AgI [30]. Silver iodide with a superionic conductivity consists of β and γ phases at room temperature which undergoes a phase transition process into the γ phase. The γ-AgI acts as a superionic conductor with high silver ionic conductivity of above 1 S cm^{-1} [31].

Herein, we evaluate the photodegradation enhancement of a novel AgI/WO_3/ZnO composite in the degradation of MB under visible light.

2. Experimental

2.1. Reagents and preparations

$Zn(NO_3)_2{\cdot}6H_2O$), ammonia, $Na_2WO_4{\cdot}2H_2O$, HNO_3, $H_2C_2O_4$, $AgNO_3$ and KI were purchased from Merck/Aldrich company. Deionized water was used throughout the study. The pH adjustment was done using HCl or NaOH solution.

For synthesis of ZnO nanosheets via a hydrothermal method, 6 mL of 25% w ammonia was added drop wise to 80 mL water containing 8 g Zn $(NO_3)_2{\cdot}6H_2O$ under continuous stirring. After 8 h, the obtained white suspension was then transferred into a 120 mL autoclave and kept at 90°C for 10 h. The obtained precipitate was separated by centrifugation (>13000 rpm) and washed several times with water and dried in air at 70°C [32].

In synthesis of WO_3 NPs, 2.5 g of $Na_2WO_4{\cdot}2H_2O$ was added to 100 mL water and dissolved by nitric acid when pH < 1. The resulted yellow tungstic acid (H_2WO_4) precipitate washed several times with water and then it was dissolved in 50 mL of 0.3 M oxalic acid solution. Finally, the clear solution was dried at 100°C and then calcined at 500°C for 2 h [33].

AgINPs were synthesized by rapid mixing of 0.25 g KI in 20 mL water (0.27 g $AgNO_3$ in 20 mL) and vigorously stirring of the suspension for 15 min. After centrifugation, it was dried during a day. The precipitate was collected, washed with water many times and then sintered at 250°C for 5 h [31].

For preparation of AgI/WO_3/ZnO composite, adequate amount of each component (for obtaining a definite mole ratio) was added in an agate mortar and hand mixed thoroughly for 5 min.

2.2. Characterization methods

XRD (X-ray diffraction) pattern was recorded by an analytical diffractometer (X'PertPro, with Ni-filtered Cu-Kα radiation at 1.5406 Å, applied potential: 40 kV, current intensity: 30 mA; Netherland). FT-IR (Fourier Transformation Infrared) spectrophotometer (PerkinElmer Spectrum 65) was used for recording FTIR spectra. UV–Vis diffuse reflectance spectrophotometer (JASCO V 670, $BaSO_4$ as reference, Japan) was used for obtaining DRS spectra. A MIRA3LMU scanning electron microscope (TESCAN Co Czech Republic) was used for study of morphology of the samples. The surface area was measured by the Belsorp mini II instrument (Microtrac Bel Corp Co., Japan). Electrochemical impedance spectra (EIS) were recorded by an Autolab instrument (PGSTAT 302, Metrohm). A pH meter/p-ion meter (Jenway model 3505) was used for the pH adjustment.

2.3. Photocatalytic performances

In a typical photocatalytic experiment, 5 mg of AgI/WO_3/ZnO photocatalyst was suspended in 10 mL 5 mg/L of MB solution. Before light irradiation, it was shaken in the dark condition for 10 min to achieve the adsorption-desorption equilibrium. After definite irradiation times by a 40 W-lamp, the withdrawn suspension was centrifuged (>13000 rpm) and the absorbance of the supernatant was recorded by a UV-Vis spectrophotometer at λ_{max} = 665 nm MB. Based on the recorded absorbance of the MB solutions before and after photodegradation process, corresponding C/C_o values were estimated. All values were averaged based on triplicate measurements (3 separate cells were irradiated simultaneously).

2.4. Preparation of samples for FTIR study

The MB solutions before and after photodegradation process (10 mL MB, 5 mg/L, and catalyst dosage 0.5 g/L)

were used for FTIR study. The samples were extracted three times with 5 mL ethyl acetate, evaporated in vacuum over anhydrous Na_2SO_4 and used for recording FTIR spectra over KBr pellets. Pure ethyl acetate was used as blank.

3. Results and discussion

3.1. Characterization of the photocatalysts

3.1.1. XRD patterns

Fig. 1 shows the XRD pattern of the as-prepared AgI/WO_3/ZnO nanostructure with some assigned peaks belong to the each constituent component. Based on literature [34], pure ZnO has XRD peaks at positions of 31.7°, 34.3°, 36.2°, 47.5°, 56.5°, 62.8° and 67.9° corresponding to the (100), (002), (101), (102), (110), (103) and (112) diffraction planes in hexagonal crystalline structure of ZnO according to JCPDS card no: 76-0704. As reported in literature [35], pure β phase AgI shows XRD peaks at 2θ values of 22.36°, 23.68°, 25.36°, 32.94°, 39.22°, 42.66° and 46.28° corresponding to *hkl* planes of (100), (002), (101), (102), (110), (103) and (112) (JCPDS No. 09-0374) [35]. Finally, XRD peaks of pure WO_3 have appeared at 2θ positions of 23.11°, 23.58°, 24.36°, 33.26°, 33.56°, 34.16°, 49.93°, 50.33°, 50.72°, 53.46°, 54.77°, 55.93°, 56.08°, 60.39°, 61.66°, and 62.26° [36]. These XRD peaks show the structural transformation from monoclinic to orthorhombic β-WO_3 structure (at 500°C) [36].

The recorded XRD pattern for the composite in this work (Fig. 1) was compared with the above mentioned peaks. Well agreement was observed between the peak positions. The recorded pattern was also compared by the instrument with the standard patterns present in its library. This comparison also showed presence of WO_3, ZnO and AgI in the composite. In the prepared XRD pattern (Fig. 1), some peaks of each component were appeared and some were overlapped, because of no pure component is present.

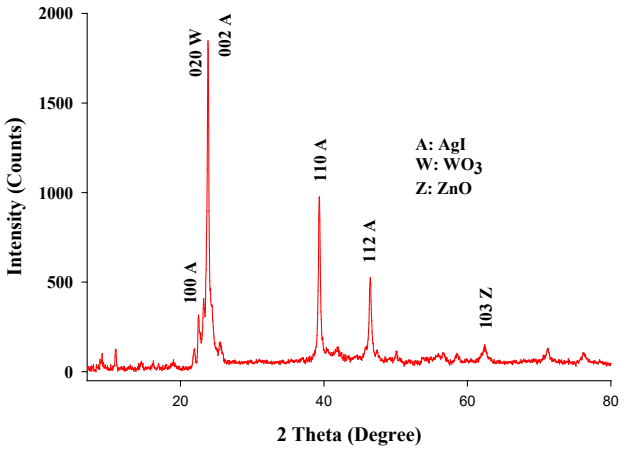

Fig. 1. XRD pattern of the as-synthesized AgI/WO_3/ZnO with mole ratio of 2:1:1.

The crystalline size of the composite was estimated about 13 nm through the following Scherrer's formula: $d = k\lambda / \beta \cos\theta$, in which λ is the Cu-Kα wavelength, β is the full width at the half-maximum (FWHM), and θ is the diffraction angle [37,38]. Some information used for this calculation are summarized in Table 1. All information used are also summarized in SDT1 (See supplementary data).

3.1.2. SEM images

To study the morphology of the as synthesized AgI/WO_3/ZnO composite, it was subjected to SEM analysis and some SEM images with different magnifications are shown in Fig. 2. Generally, the composite has nano-dimension as obvious in image-A. The images contained some nano-sheets, nano-rods and nano-particles. It has reported that hydrothermal synthesis of ZnO at shorter times gave ZnO NPs. When hydrothermal duration increased to about 10 h (applied in the present work), ZnO NPs could aggregate and assemble in one-dimensional order to form the ZnO nano-sheets. At this condition, some nano-rods may be formed which may be completed at longer heating times about 14 h [32]. Some nano-sheets may relate to WO_3 species. Based on literature [36], WO_3 formed randomly oriented sheet-like structure that its thickness was about a few tens nm while its width was about a few μm. The nanoparticles belong to AgI ingredient [31]. Formation of nano-sheets is also important because it increases the effective surface area of the catalyst which in turn increase the photocatalytic activity. Typical EDX spectrum of the composite is shown in Fig. 2D. As shown, all constituent elements of the composite were appeared in the spectrum. The quantitative results of this analysis is also shown in SDT2. The corresponding percentages of each composite component are summarized in this table. The results do not have a precise agreement with the mole ratio of 2:1:1 for the AgI/WO_3/ZnO composite, because EDX is a semi-quantitative and spot test analysis technique which analyses a small point of the sample.

3.1.3. DRS studies

Fig. 3 shows typical absorption spectra of the single and coupled semiconductors obtained in diffuse reflectance spectroscopy study of the samples. The absorption edge wavelengths were determined about 369, 410, 448 and

Table 1
XRD information used for the estimation of the crystallite size of the composite by Scherrer equation

θ (o)	FWHM	β	cos θ	β cosθ	*d* (nm)	Average *d* (nm)
10.97	0.2952	0.0121	0.98	0.0119	11.64	13.08
11.93	0.1986	8.1625e-3	0.98	7.9862e-3	17.36	
12.77	0.3936	0.0162	0.98	0.0158	8.78	
19.68	0.2460	0.0101	0.94	9.52e-3	14.56	

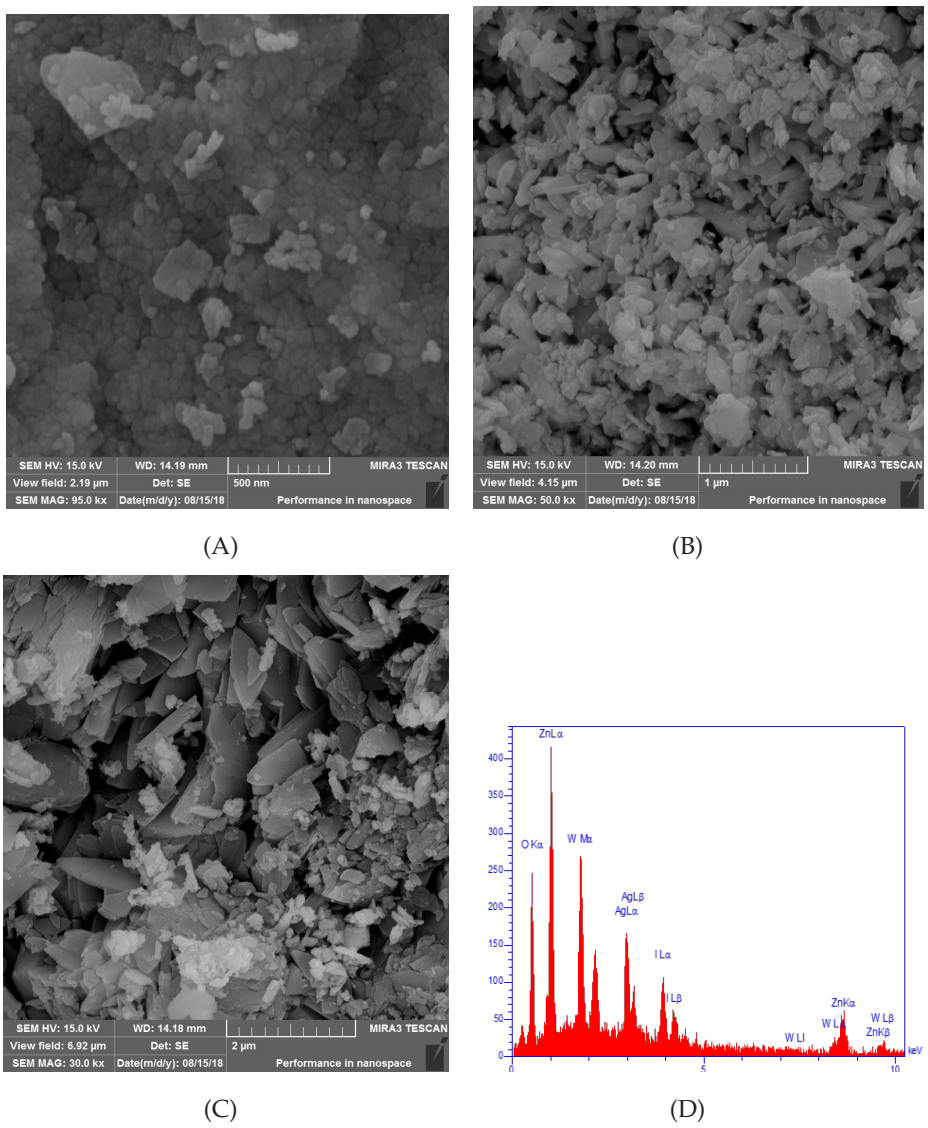

Fig. 2. Some SEM images of the as-synthesized AgI/WO_3/ZnO with mole ratio of 2:1:1 (A–C); (D) Typical EDX spectrum of the composite.

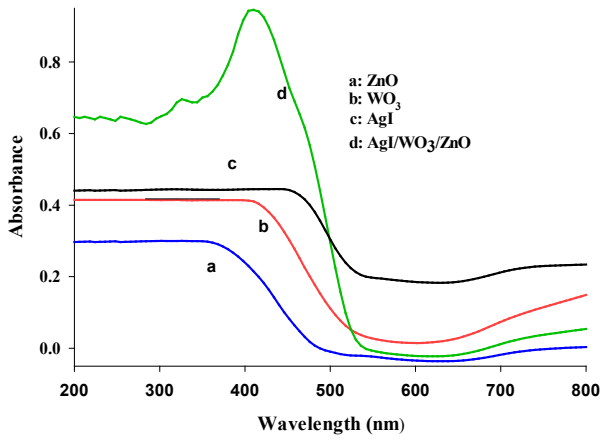

Fig. 3. The absorption spectra of single AgI, WO_3, ZnO and the AgI/WO_3/ZnO semiconductors obtained in DRS technique.

417 nm for ZnO, WO_3, AgI and the composite, respectively. These values were substituted in $1240/\lambda_{onset}$ equation to calculate the band gap energy (in eV) of each sample [39,40]. In addition, electronegativity of each sample was used for the calculation of potential position of the V_b and C_b of the semiconductors. All information used for these calculations and the obtained results are summarized in Tables 2 and 3. The band gap energy of single AgI, WO_3 and ZnO was found to be 2.97 eV, 2.91 eV and 3.36 eV, respectively, while the value of 2.97 eV was obtained for the AgI/WO_3/ZnO composite. In general, the composite showed a red shift in band gap energy with respect to single ZnO semiconductor. Comparison of the band gaps with that of the corresponding bulk semiconductors in Table 3 [41–43], confirms a blue shift in band gaps of used semiconductors. Generally, nano-particles have higher band gap energies with respect to the bulk systems.

The following empirical formula was used to determine the V_B position of the used semiconductors in order to clar-

Table 2
Mulliken electronegativity of the constituent elements of the used semiconductors by using their electron affinity (E_a) and the first ionization energy (E_i) in eV

Element	E_a (eV)	E_i (eV)	½(E_a + E_i) (eV)
Zn	–0.600	9.394	4.397
O	1.461	13.618	7.490
Ag	1.304	7.576	4.440
I	3.059	10.451	6.755
W	0.816	7.864	4.380

Table 3
Band gap energies and potential positions of V_B and C_B of the used semiconductors of the composite by using empirical formula of $E_{VB} = X - E_O + 0.5\,Eg$. X data are in Mulliken's electronegativity scale [50–54]

Catalyst	X eV	Eg (eV)	Eg bulk(eV)	V_B (eV)	C_B (eV)
AgI	5.48	2.97	2.83	2.465	– 0.505
WO_3	6.54	2.91	2.75	3.495	0.585
ZnO	5.76	3.36	3.20	2.940	– 0.420
Composite	–	2.97	–	–	–

ify the charge transport in the interfaces. In this formula, E_{VB}, E_g, X and E_e are the V_B edge potential, the band gap energy of the semiconductor, the geometric mean of the electronegativity of the constituent atoms in the investigated semiconductor and E_e is the energy of free electrons relative to the normal hydrogen electrode (about 4.5 eV), respectively [44–48]:

$$E_{VB} = X - E_e + 0.5\,E_g \quad (1)$$

The electronegativity of the used semiconductors can be estimated by half value of summation of the first ionization energy (E_i) and the electron affinity (E_a) of the element [49]. All results are summarized in Table 2, All reported data have adopted from literature [50–54].

By using the aforementioned formula, E_{VB} was calculated and used for the estimation of E_{CB} by using $E_{CB} = E_{VB} - E_g$ formula [55]. All results are summarized in Table 3. The resulted potential positions were then used to draw the Schematic energy diagram to illustrate the charge carriers' transfer in the composite as shown in next sections (see photodegradation section).

3.1.4. Photoluminescence spectra

As we know, recombination of the photogenerated e^-/h^+ pairs is a most important drawback of the semiconducting based photodegradation processes that significantly limits its efficiency. This also increases the cost of the method. In contrast, the most famous and common method to study the recombination rate of the photogenerated e^-/h^+ pairs is photoluminescence (PL) spectroscopy [56]. Hence, photoluminescence of the single AgI, ZnO and WO_3 semiconductor NPs and their corresponding ternary composite (in acetone dispersion) were recorded which of results are shown in Fig. 4. For all samples, when the suspensions were irradiated at 350 nm, typical emission peaks were appeared at 484 nm and about 700 nm. The most important point that can be adopted from the spectra is significant decrease in PL intensity of the composite with respect to the single semiconductors. This confirms that the rate of the recombined e^-/h^+ pairs is low in the composite due to a better charge carriers' transference occurred between the coupled semiconductors. Hence, a maximum photodegradation rate would be expected for this composite system which of results will discuss in the photodegradation sections.

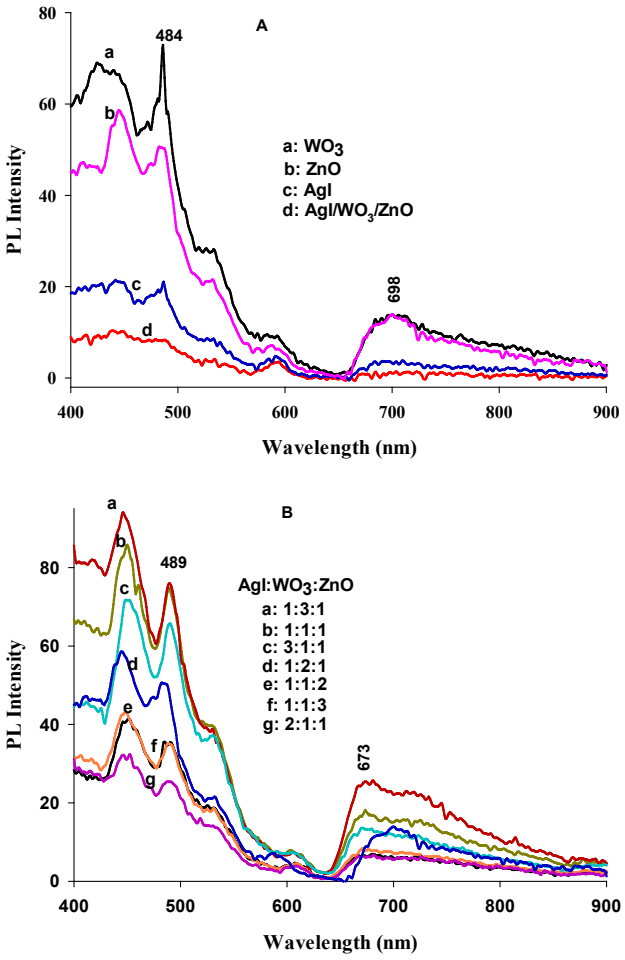

Fig. 4. (A) Photoluminescence (PL) spectra of the as synthesized samples in acetone (sample preparation: 1mg catalyst in 20 mL acetone was dispersed by ultrasonication for 30 minutes), (B) PL spectra of the AgI/WO_3/ZnO composite as a function of mole of the components in conditions similar to case A.

As shown in Fig. 4B, PL intensity depends on the mole ratio of the coupled semiconductors. The lowest PL intensity was observed for 2:1:1 < 1:2:1 < 1:3:1 mole ratios of AgI/WO_3/ZnO, respectively. As will show in the photodegradation section, the best photocatalytic activity was appeared for these catalysts. This confirms that the charge carriers' transference in the composite depends on the ratio of the coupled ingredients. This means that more •OH radicals can generate by the AgI/WO_3/ZnO composite system than

that of single catalysts. This counts as an important advantage of the photocatalytic activity of composite systems with respect to the single components [57].

3.1.5. Study of surface charge of the catalysts

Generally, colloids and suspended matters in water can sorb charged particles present in the contact solution due to an electrostatically effect. Thus, the higher the charge and concentration of the counter ion in the contacted solution cause to the higher adsorbed ions. This instantaneous and reversible process takes place at a stoichiometric ratio and retains the electro-neutrality of the system. In addition, counter ions for the main ions in solution has also a vital role on the adsorption extent of the main ion. Hence, the surface charge of the adsorbent plays a pivotal role on the adsorption phenomena. Because a catalytic process takes place on the surface of the catalyst, the adsorption extent of the analyte is very important for such process. The aforementioned facts can be discussed with more details based on the point of zero charge pH (pHpzc, or the simply, pzc), at which the catalyst/adsorbent surface has a net zero charge neutralized by the surrounded solution. At this point, total charge adsorbed at the surface of the catalyst/adsorbent (including all the cations and anions) is zero [58,59].

Based on this discussion, it would be concluded that, the initial pH of the solution determines the type of exchange/adsorption as illustrated below. (i) At pH below pH_{pzc}, the surface has a net positive charge and contains excess protons. Thus, the particles can exchange or adsorb anionic materials. (ii) At pH equal to pH_{pzc}, a net zero charge is present on the surface because it is balanced with protons and hydroxyls. There is no exchange capacity at this point. (iii) At pH higher than pH_{pzc}, the excess of dissociated hydroxyl negative groups are present on the surface, resulting a net negative charge on the surface and a cation exchange property. At these pHs, the surface is capable to adsorb cationic materials.

Generally, in pH ranges that both the adsorbate species and adsorbent surface have the same charge, the resulted repulsive force between them causes to a relatively weak adsorption. In contrast, under certain conditions ($pH_{pzc} > pK_a$ for acids; $pH_{pzc} < pK_a$ for bases) there are pH ranges in which the adsorbate species and adsorbent surface have opposite charges, causing an attraction force between the adsorbate and the surface. These attraction forces together with Van der Waals forces create a maximum adsorption capacity in these pH ranges [60].

To determine the pH_{pzc} value for as-synthesized catalysts, some suspensions containing 0.1 g of each catalyst in 10 mL 0.2 M NaCl were prepared and their initial pHs (pH_I) were adjusted in range of 2–10. The suspensions were shaken at 250 rpm at room temperature for 24 h and their final pH (pH_F) were recorded [61]. The plot of pH_F–pH_I was drawn (Fig. 5) and intersection of each plot with the bisector of the curve (plot of pH_I vs pH_I) was recorded as the pH_{PZC} for each catalyst. The values of 6.23, 5.25, 7.25 and 6.23 were obtained for pH_{pzc} of AgI, WO_3, ZnO and AgI/WO_3/ZnO, respectively.

3.1.6. Surface area study

The BET (Brunauer-Emmett-Teller) surface area of the as-synthesized compounds was investigated via nitrogen adsorption-desorption isotherms which of results are presented in Fig. 6A. By using the BET equation, S_{BET} was determined from the isotherms. The results are summarized in Table 4. The results shows an increased specific surface area of the as-synthesized ternary nano-composite compared with the mono-component systems. This increased surface area provides more active sites for charge carriers' transfer and their accumulation for the ternary composite. This in turn can cause to an enhanced photocatalytic activity for the composite [62]. Generally, it has reported when the BET surface area for WO_3 nano-plates compared with that of WO_3 nano-rods, a higher surface area has observed for nano-plates. This has related to presence of more edges and faces in nano-plates due to its especial geometric shape [63]. Usually, the particles having smaller pores also have a larger effective surface area but the surface area of particles depends also on its porosity (the number of pores on one gram of the particles). In some cases, there may be a particle having very small pores but only a small number of pores and hence a small specific surface area [64].

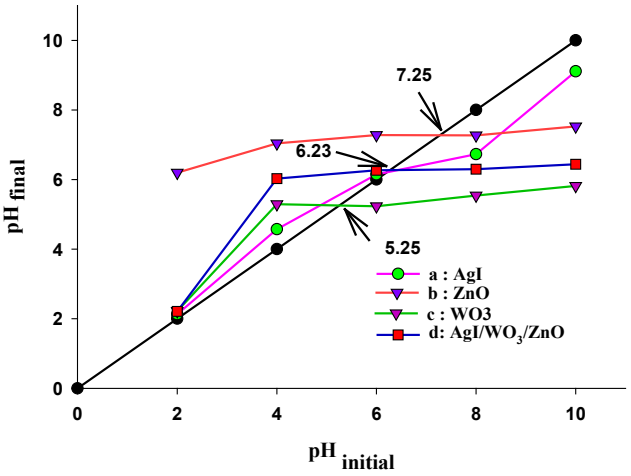

Fig. 5. Typical plots of pH_F–pH_I used for the estimation of pH_{pzc} for single AgI, WO_3 and ZnO semiconductors and the corresponding AgI/WO_3/ZnO composite(mole ratio of AgI/WO_3/ZnO was 2:1:1).

3.1.7. Electrochemical impedance spectroscopy (EIS)

The EIS spectra of the single and the composite systems were recorded to evaluate the charge transfer ability of the modified carbon paste electrode (CPE) by the samples. The modified electrode was constructed by the typical procedure reported in literature [65], at which a good discussion on EIS spectra has illustrated. The resulted Nyquist plots are summarized in Fig. 6B. Generally, a smaller arc radius of the Nyquist plots means that a smaller electrical resistivity is present in the electrode. This results a higher charge transfer for the investigated electrode [66–68]. The following trend was observed for arc radius of the Nyquist plots for the modified electrode with the used samples:

WO_3 > AgI > ZnO > WO_3-AgI-ZnO

This confirms a better charge transfer for the composite system that could result a higher photodegradation activity for it.

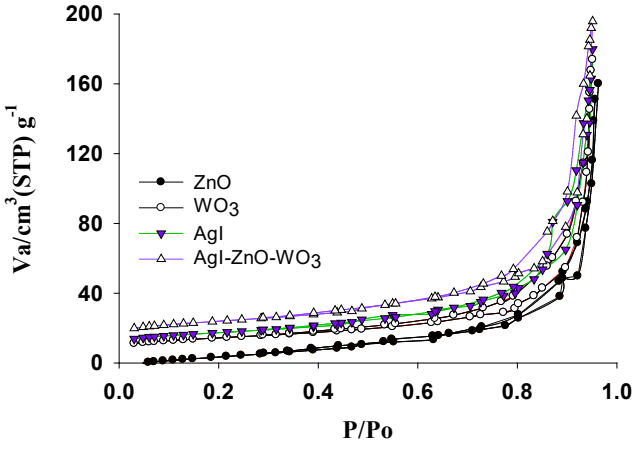

(A)

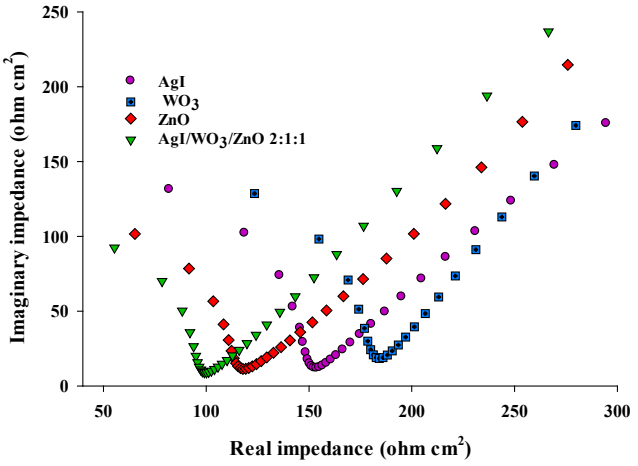

(B)

Fig. 6. (A) Typical N_2 adsorption-desorption isotherms and (B) the EIS Nyqusit plots (CPE modified contains 20% of each modifier, Amplitude: 10.0 mV, Frequency: 10 mHz to 100 kHz, Electrolyte: 0.1 M Na_2SO_4, Potential: 0.0 V versus Ag/AgCl, Counter electrode: Pt) of the synthesized samples.

Table 4
Some information obtained in BET study of the samples

Sample	S_{BET} (m^2/g)	Avr. pore size (nm)
ZnO	22.45	2.43
WO_3	36.28	2.18
AgI	38.80	1.85
AgI-WO_3-ZnO	52.41	1.12

3.2. Photodegradation experiments

3.2.1. Initial removal and photodegradation experiments

Decrease in MB concentration by surface adsorption, direct photolysis and photocatalytic degradation processes was followed by change in the UV-Vis absorption spectra of the corresponding solutions as shown in Fig. 7A. As indicated, absorbance of MB solution at its λ_{max} (665 nm) was decreased during the aforementioned processes. Change in the UV-Vis absorbance of MB solution as a function of its monomer, dimer and trimer has been comprehensively discussed in literature [69]. According to the results, direct photolysis removed low amounts of MB molecules, confirming the good stability of MB molecules at the applied conditions. Surface adsorption also removed little MB molecules. To eliminate its role on the photodegaradtion process, before irradiation process all suspensions were shaken at dark for 10 min. As results show, during the photocatalytic degradation process by the single and composite catalysts removed MB was increased, especially in case of the composite with AgI/WO_3/ZnO mole ratio of 2:1:1.

As mentioned in section 3.1.3, the band gaps of AgI, WO_3, ZnO and AgI/WO_3/ZnO are about 2.87 eV, 2.67 eV, 2.61 eV and 2.62 eV, respectively. Theoretically, all the used catalysts can be excited under irradiated photons and participate in the photocatalytic degradation process. But, the trend of AgI > WO_3 > ZnO was observed in the photocatalytic ability of the single semiconductors, which can be related to the phase crystallinity of the semiconductors, because photoactivity of semiconductors significantly depends on their crystallite phase structures [70].

The boosted photocatalytic activity of the composite with respect to the single systems is due to increased charge carriers' separation in the composite system as it was illustrated in the typical schematic diagram in Fig. 7B. The diagram is a "cascade" type (also known as a domino reaction or tandem reaction that is common in organic chemistry) electron/hole transfer. The photogenerated electrons in conduction band of AgI (C_b-AgI) have a more negative E^o-value than the C_b-ZnO level and hence can rapidly immigrate to the C_b-ZnO level before they can recombine with the holes in the V_b-AgI level. Similarly, such process can occur from the C_b-ZnO level to the C_b-WO_3 level because of suitable matching of their E^o-values for occurring internal redox process between them. Such charge transfer process, significantly decreases the e^-/h^+ recombination process. The aforementioned electrons in the C_b-AgI level and the C_b-ZnO level have more negative potentials than $O_2/{}^{\bullet}O_2$ and hence they can reduce dissolved oxygen to super oxide radicals. But the electrons in the C_b-WO_3 level cannot do this process and they may directly reduce MB molecules. In the other way, the photogenerated holes in the V_b-ZnO and V_b-WO_3 levels have suitable E^o-values for oxidizing hydroxyl anions to hydroxyl radicals ($E^o{}^{\bullet}OH/OH^-$: 2.73 V). MB has the E^o value of 0.011 V [71] and hence it can be oxidized by the holes in the V_b-levels of all the coupled semiconductors of the composite [72–74].

Based on the aforementioned discussion and results, it would be concluded that mole ratio of the combined semiconductors of the composite, can play an important role to prevent the e^-/h^+ recombination and increasing the photodegradation activity of the resulted composites. Results of this study are shown in Fig. 7C. The results confirm that when the mole ratio of AgI in the composite is twice than the other ingredients, the best degradation efficiency was obtained. This confirms that a good charge transfer between the included semiconductors of the composite was occurred in this mole ratio. Thus, when much photogenerated e^-/h^+ pairs produced in the AgI and ZnO levels, rapid charge

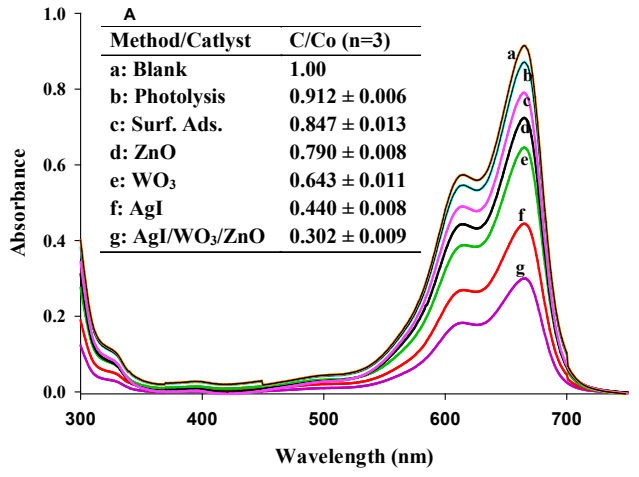

(A)

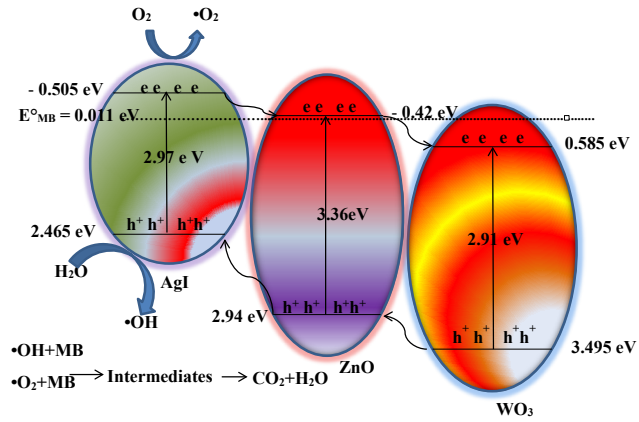

(B)

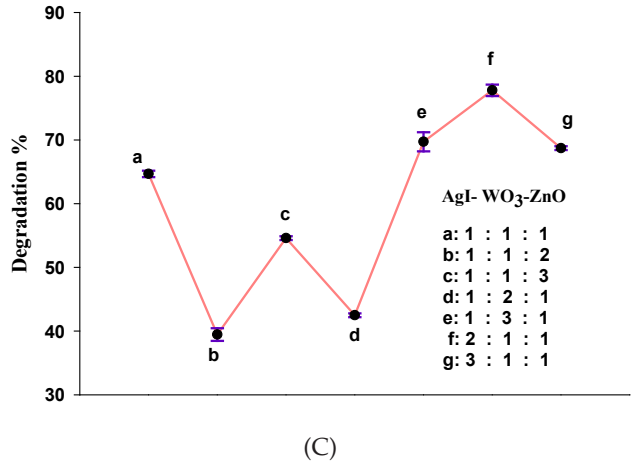

(C)

Fig. 7. (A) Decrease in UV-Vis absorption spectra of MB solution during its photodegradation by pure AgI, WO_3, ZnO and AgI/WO_3/ZnO catalyst (5 mg of each catalyst in 10 mL of 5 mg/L MB, mole ratio of AgI/WO_3/ZnO was 2:1:1 during 40 min); (B) The schematic illustration of photocatalytic mechanism for the ternary AgI/WO_3/ZnO system; (C) The photodegradation results obtained in MB degradation as a function of mole ratio of the composite ingredients (7 mg of each catalyst in 10 mL of 5 mg/L MB, time: 40 min).

transfer diminished the e^-/h^+ recombination and hence the photoactivity of the resulted composite was increased. Hence, the composite with this mole ratio was used in next steps and for characterization experiments.

3.2.2. FT-IR spectra

FTIR spectra of MB solution before and after photodegradation experiments were recorded which of results are shown in Fig. 8. In spectrum of untreated MB, the stretching vibration of -CH- aromatic and -CH_3 methyl groups showed an absorption peak at 3001 cm^{-1}. The absorption peak at about 1480 cm^{-1} is also related to the -CH_3 stretching absorption. The vibrations of –C–C– bond showed peaks at about 1066 cm^{-1} [75]. Comparison of MB spectra shows appearance of new peaks at 3452 cm^{-1} and 1655 cm^{-1}. The first ones corresponds to elongation of OH, vibration modes of inter and intramolecular hydrogen bonding of degradation intermediates such as alcohols, phenols, carboxylic acids etc. formed during the degradation of MB molecules. The second new peak which appeared at 1655 cm^{-1} can be related to the asymmetric stretching vibration of –C=O. Appearance of such peaks for MB sample after the photodegradation process confirms formation of some degradation intermediates such as carboxylic acid. No further attempts were done for detection of the intermediates.

3.2.3. Kinetic aspect of the process

In general, the Langmuir-Hinshelwood (L-H) method is the best and common method to model the kinetic of a heterogeneous photodegradation process which relates to the adsorption of pollutants onto the surface of the catalysts. The L-H model is based on monolayer adsorption of the pollutants onto the catalyst (adsorbent) surface. This is important because of a catalytic process occurs on the cata-

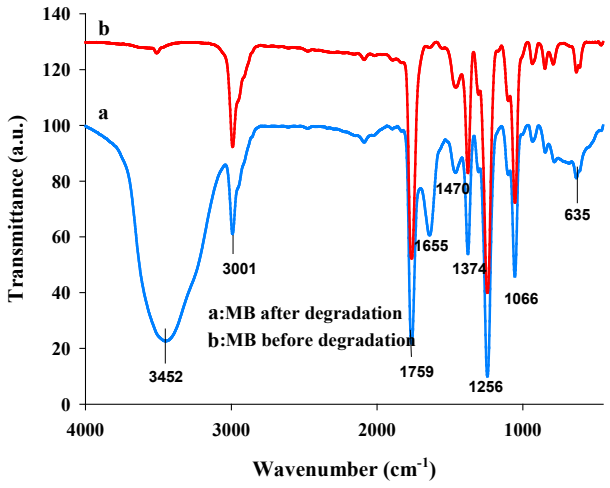

Fig. 8. FTIR spectra of MB sample before and after photodegradation process (Irradiation condition: 5 mg AgI/WO_3/ZnO with mole ratio of 2:1:1 in 10 mL 5 mg/L MB irradiated for 40 min; FTIR measurements were done by three times extraction with 5 mL of ethyl acetate, evaporated in vacuum over anhydrous Na_2SO_4 and one drop was used over KBr pellets).

lyst surface. General equation for describing the kinetic of the process by the L-H model is shown in Eq. (2), in which the reaction rate r (mg/L min) depends on k (the specific reaction rate constant in mg/L min), K (the equilibrium constant of the reactant in L/mg) and C (pollutant concentration).

$$r = -dC/dt = (kKC)/(1+KC) = k'\theta \quad (2)$$

$$\ln (C_o/C) + k(C_o - C_t) = kKt = k \times t \quad (3)$$

The logarithmic form of the L-H equation is shown by Eq. (3) in which C_o, C_t, t and k show the initial and final concentrations of the investigated pollutant, irradiation time and the apparent first-order rate constant, respectively. At high concentrations (C > 5 mM) Eq. (2) shows a zero order-kinetic process but when C < 1 mM, an apparent first-order kinetic model can be obtained for the reaction as shown by Eq. (3) [76–78].

To follow the kinetic of the process, some experiments were done and the plot of $\ln(C/C_o)$ versus irradiation time was constructed. As shown in Fig. 9A, the rate constant of 0.025 min^{-1} was obtained for the degradation of MB by the proposed catalyst at the applied conditions. The amount of 0.997 for R^2 confirms a good fitting of the data by the L-H model. Based on the results, about 70% of MB molecules were degraded during 40 min photodegradation process.

3.2.4. Chemical oxygen demand (COD)

In general, to follow the mineralization extent of an investigated pollutant, COD is a useful method that it values state as mg O_2/L. This method provides a measure of the required oxygen need for the degradation of an organic pollutant present in media. Thus, a higher COD confirms a higher polluted water. COD values of MB solution before and after photodegradation process at different irradiation times were determined and the results are shown in Fig. 9B. As shown, the COD values of 202,172, 146, 133, 124, 120, and 118 mg O_2/L were obtained for irradiation times of 0, 15, 30, 45, 60, 75 and 90 min. Comparison of the initial and final COD values confirms about 42% of MB molecules were degraded during 90 min, which is smaller than the values obtained by UV-Vis absorption spectroscopy. This shows that MB molecules may formed degradation intermediates that have not enough absorbance in λ_{max} MB causing a decrease in the recorded absorbance. Hence, a higher degradation extant was obtained. But, the COD results show the mineralized MB molecules. Fig. 9C shows typical curve plotted based on COD results to study the kinetic of the process. As shown, the rate constant of 0.055 min^{-1} was obtained. This shows mineralization rate of MB molecules is 2.2 times greater than the degradation extent obtained by the UV-Vis results (k = 0.025 min^{-1}).

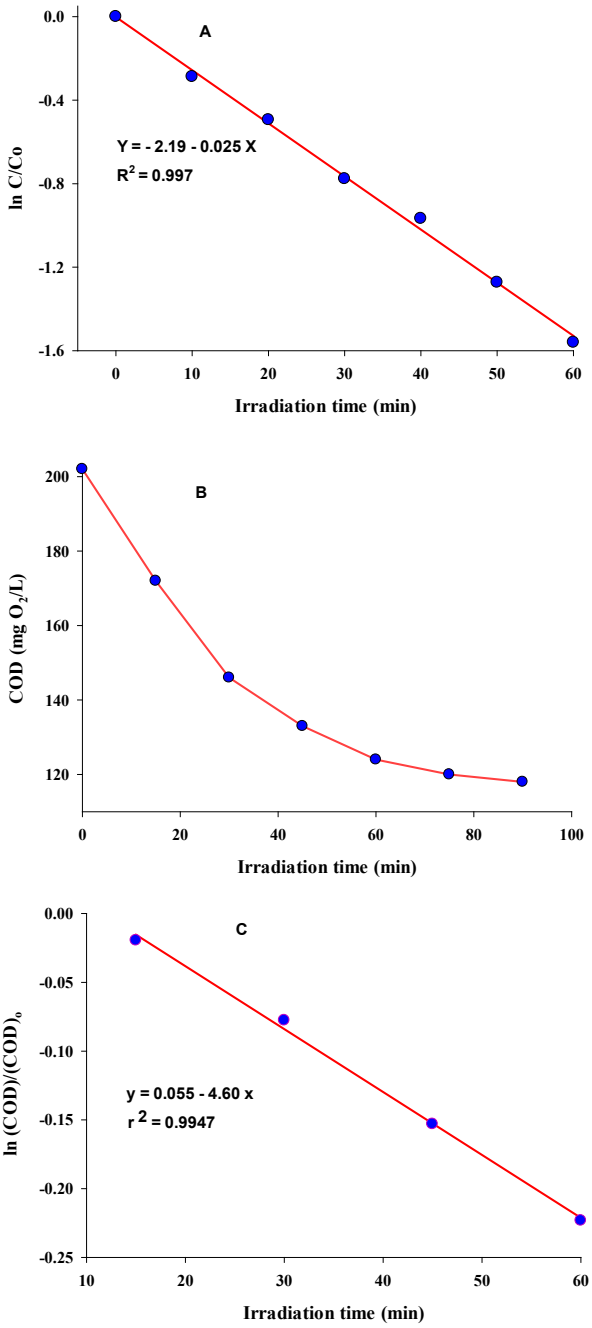

Fig. 9. A) Typical ln C/C_o plots *vs* irradiation time for the calculation of k-value in degradation of MB by AgI/WO_3/ZnO catalyst (MB = 5 mg L^{-1}, pH 5, amount of the catalyst = 0.5 g/L. with mole ratio of 2:1:1); B) COD values of MB solution during the photodegrdation process (conditions are same as case A); C) Typical plot of ln (COD/COD_o) versus irradiation time for study the kinetic of the process.

3.2.5. Reuse of the photocatalyst

Economically and environmentally, applicability of a novel catalyst in successive re-using runs without striking decrease in its activity is a prime importance [79]. This important advantage was done for the proposed catalyst by subjecting it in the photodegradation of MB in the optimized conditions. After each run, the catalyst was separated and dried at 100°C for 30 min and then used in the next run. The obtained results are shown in Fig. 10. As shown, the reused catalyst showed good activity after 4 reusing runs and after this run 10% of its initial activity was loosed.

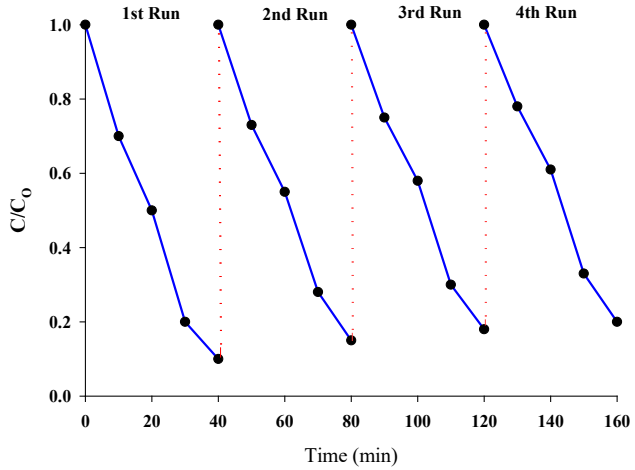

Fig. 10. Reuse ability of the photocatalyst during 4 runs. (Irradiation conditions: [MB] = 5 mg/L, pH 5, catalyst dosage = 1.0 g/L, drying process: 30 min at 100°C).

4. Conclusion

The results confirmed that coupling of AgI, WO_3 and ZnO nanoparticles can cause to a boosted activity in their photocatalytic activities in the photodegradation of MB aqueous solution. This increased activity agree with the results obtained by PL spectroscopy, because the resulted composite showed a lower PL intensity than the mono-component systems. This lower PL intensity shows a lower e^-/h^+ recombination and hence a higher charge carriers' transfer in the composite. The PL intensity, and hence the photocatalytic activity, depend on the mole ratio of the ingredients in the composite. Thus, a better photodegradation activity was obtained for the AgI/WO_3/ZnO composite with a mole ratio of 2:1:1. This composite also had the lowest PL intensity than the other composites with different mole ratios. The rate constants of 0.055 and 0.025 were obtained by the COD and UV-Vis results, confirming the mineralization rate of MB is 2.2 times greater than the degradation extent.

References:

[1] T.W. Hartley, Public perception and participation in water reuse, Desalination, 187 (2006) 115–126.
[2] M.H. Plumlee, J. Larabee, M. Reinhard, Perfluorochemicals in water reuse, Chemosphere, 72 (2008) 1541–1547.
[3] M. Pirhashemi, A. Habibi-Yangjeh, Sh. Rahim Pouran, Review on the criteria anticipated for the fabrication of highly efficient ZnO-based visible-light-driven photocatalysts, J. Ind. Eng. Chem., 62 (2018) 1–25.
[4] M. Bordbar, Seyed M. Vasegh, S. Jafari, A. Yeganeh Faal, Optical and photocatalytic properties undoped and Mn-doped ZnO nanoparticles synthesized by hydrothermal method: Effect of annealing temperature, Iranian J. Catal., 5 (2015) 135–141.
[5] H. Guoa, K-l. Lin, Z-sh. Zheng, F-b. Xiao, Sh-x. Li, Sulfanilic acid-modified P25 TiO_2 nanoparticles with improved photocatalytic degradation on Congo red under visible light, Dyes Pigments, 92 (2012) 1278–1284.
[6] B.A. Ünnü, G. Gündüz, M. Dükkancı Heterogeneous Fenton-like oxidation of crystal violet using an iron loaded ZSM-5 zeolite, Desal. Water Treat., 57 (2016) 11835–11849.
[7] M. Karimi-Shamsabadi, M. Behpour, A. KazemiBabaheidari, Z. Saberi, Efficiently enhancing photocatalytic activity of NiO-ZnO doped onto nanozeoliteX by synergistic effects of p-n heterojunction, supporting and zeolite nanoparticles in photo-degradation of Eriochrome Black T and Methyl Orange, J. Photochem. Photobiol. A: Chem., 346 (2017) 133–143.
[8] J.-L. Capelo-Martínez, P. Ximénez-Embún, Y. Madrid, C. Camara, Advanced oxidation processes for sample treatment in atomic spectrometry, Trac. Trend. Anal. Chem., 23 (2004) 331–340.
[9] S. Landi Jr, J. Carneiro, S. Ferdov, António M. Fonseca, Isabel C. Neves, M. Ferreira, P. Parpot, Olivia S.G.P. Soares, Manuel F.R. Pereira, Photocatalytic degradation of Rhodamine B dye by cotton textile coated with SiO_2-TiO_2 and SiO_2-TiO_2-HY composites, J. Photochem. Photobiol. A: Chem., 346 (2017) 60–69.
[10] S. Mousavi-Mortazavi, A. Nezamzadeh-Ejhieh, Supported iron oxide onto an Iranian clinoptilolite as a heterogeneous catalyst for photodegradation of furfural in a wastewater sample, Desal. Water Treat., 57 (2016) 10802–10814.
[11] H. Che, G Che, E. Jiang, Ch. Liu, H. Dong, Ch. Li, A novel Z-Scheme CdS/Bi_3O_4 Cl heterostructure for photocatalytic degradation of antibiotics: Mineralization activity, degradation pathways and mechanism insight, J. Taiwan Institute Chem. Eng., 000 (2018) 1–11.
[12] S. DharmrajKhairnar, M. Rajendra Patil, V. Shankar Shrivastava, Hydrothermally synthesized nanocrystalline Nb_2O_5 and its visible-light photocatalytic activity for the degradation of congo red and methylene blue, Iranian J. Catal., 2 (2018) 143–150.
[13] Zarifeh-AlsadatMirian, A. Nezamzadeh-Ejhieh, Removal of phenol content of an industrial wastewater via a heterogeneous photodegradation process using supported FeO onto nanoparticles of Iranian clinoptilolite, Desal. Water Treat., 57 (2016) 16483–16494.
[14] Mingbei Zhu, Yunxia Li, Shouqin Tian, Y. Xie, Xiujian Zhao, X. Gong, Deep-red emitting zinc and aluminium co-doped copper indium sulfide quantum dots for luminescent solar concentrators, J. Colloid Interf. Sci., 534 (2019) 509–517.
[15] B. Khodadadi, Effects of Ag, Nd codoping on structural, optical and photocatalytic properties of TiO_2 nanocomposite synthesized via sol-gel method using starch as a green additive, Iran. J. Catal., 6 (2016) 305–311.
[16] M. Shekofteh-Gohari, A. Habibi-Yangjeh, M. Abitorabi, A. Rouhi, Magnetically separable nanocomposites based on ZnO and their applications in photocatalytic processes: A review, Critical Rev. Environ. Sci. Techn., 48 (2018) 806–857.
[17] Chongyang Liu, Jinze Li, Linlin Sun, Yaju Zhou, Chun Liu, Huiqin Wang, PengweiHuo, Changchang Ma, Yongsheng Yan, Visible-light driven photocatalyst of CdTe/CdS homologous heterojunction on N-rGO photocatalyst for efficient degradation of 2,4-dichlorophenol, J. Taiwan Inst. Chem. Eng., 93 (2018) 603–615.
[18] P. Raizada, J. Kumari, P. Shandilya, P. Singh, Kinetics of photocatalytic mineralization of oxytetracycline and ampicillin using activated carbon supported ZnO/$ZnWO_4$ nanocomposite in simulated wastewater, Desal. Water Treat., 79 (2017) 204–213.
[19] A. Nezamzadeh-Ejhieh, M. Bahrami, Investigation of the photocatalytic activity of supported ZnO-TiO_2 on clinoptilolite nano-particles towards photodegradation of wastewater-contained phenol, Desal. Water Treat., 55 (2015) 1096–1104.
[20] N. Masoudipour, M. Sadeghi, F. Mohammadi-Moghadam, Photo-catalytic inactivation of E. coli using stabilized Ag/S, N-TiO_2 nanoparticles by fixed bed photo-reactor under visible light and sunlight, Desal. Water Treat., 110 (2018) 109–116.
[21] S. Dianat, Visible light induced photocatalytic degradation of direct red 23 and direct brown 166 by $InVO_4$-TiO_2 nanocomposite, Iran. J. Catal., 8(2) (2018) 121–132.
[22] Praveen K. Surolia, Raksh V. Jasra, Photocatalytic degradation of p-nitrotoluene (PNT) using TiO_2-modified silver-exchanged NaY zeolite: kinetic study and identification of mineralization pathway, Desal. Water Treat., 57 (2016) 22081–22098.
[23] M. Mousavi, A. Habibi-Yangjeh, Sh. Rahim Pouran, Review on magnetically separable graphitic carbon nitride-based nanocomposites as promising visible-light-driven photocatalysts, J. Mater. Sci: Mater. Electron., 29 (2018) 1719–1747.

[24] K. Choi, T. Kang, S-G. Oh, Preparation of disk shaped ZnO particles using surfactant and their PL properties, Mater. Lett., 75 (2012) 240–243.
[25] Gh. Ahangar, E. Abbaspour-Fard, N. Shahtahmassebi, M. Khojastehpour, P. Maddahi, Preparation and characterization of PVA/ZnO nanocomposite, J. Food Proc. Preserv., 39 (2015) 1442–1451.
[26] C-B. Ong, L-Y. Ng, A-W. Mohammadad A review of ZnO nanoparticles as solar photocatalysts: Synthesis, mechanisms and applications, Renew. Sust. Energy Rev., 81 (2018) 536–551.
[27] M. Al-Fori, S. Dobretsov, MTZ. Myint, J. Dutta, Antifouling properties of zinc oxide Nano rod coatings, Biofouling, 30 (2014) 871–882.
[28] S. Aghdasi, M. Shokri, Photocatalytic degradation of ciprofloxacin in the presence of synthesized ZnO nanocatalyst: The effect of operational parameters, Iran. J. Catal., 6 (2016) 481–487.
[29] S.-G. Kumar, R. Koteswara, K. Rao, Comparison of modification strategies towards enhanced charge carrier separation and photocatalytic degradation activity of metal oxide semiconductors (TiO_2, WO_3 and ZnO), Appl. Surf. Sci., 391 (2017) 124–148.
[30] Fenglin Liu, Xianjie Chen, Qinghua Xia, Lihong Tian, Xiaobo Chen, Ultrathin tungsten oxide nanowires: oleylamine assisted nonhydrolytic growth, oxygen vacancy and high photocatalytic properties, RSC. Adv., 5 (2015) 77423–77428.
[31] N-L. Hawari, M-R. Johan, Synthesis and characterizations of AgI nanoparticles via mechanochemical reaction, J. Alloy. Compd., 509 (2011) 2001–2006.
[32] N. Elamin, A. Elsanousi, Synthesis of ZnO nanostructures and their photocatalytic activity, J. Appl. Ind. Sci, 1 (2013) 32–35.
[33] M. Farhadian, P. SangpourGh. Hosseinzadeh, Preparation and photocatalytic activity of WO_3-MWCNT nanocomposite for degradation of naphthalene under visible light irradiation, RSC. Adv., 00 (2016) 1–11.
[34] J. Safaei-ghomi, M.-A. Ghasemzadeh, Silver iodide nanoparticle as an efficient and reusable catalyst for the one-pot synthesis of benzofurans under aqueous conditions, J. Chem. Sci., 125 (2013) 1003–1008.
[35] Sh. Yamasaki, T. Yamada, H. Kobayashi, H. Kitagawa, Preparation of sub-10 nm AgI nanoparticles and a study on their phase transition temperature, Chem. Asian J., 8 (2013) 73–75.
[36] S.V. Prabhakar Vattikuti, Ch. Byon, I-L. Ngo, Highly crystalline multi-layered WO_3 sheets for photodegradation of Congo red under visible light irradiation, Mater. Res. Bull., 84 (2016) 288–297.
[37] Sh. Aghabeygi, R. Kia Kojoori, H. Vakili Azad, Sonosynthesis, characterization and photocatalytic degradation property of nanoZnO/zeoliteA, Iran. J. Catal., 6 (2016) 275–279.
[38] M. Khatamian, M. Irani, Preparation and characterization of nanosized ZSM-5 zeolite using kaolin and investigation of kaolin content, crystallization time and temperature changes on the size and crystallinity of products, J. Iran. Chem. Soc., 6 (2009) 187–194.
[39] M. Pirhashemi, A. Habibi-Yangjeh, Preparation of novel nanocomposites by deposition of Ag_2WO_4 and AgI over ZnO particles: Efficient plasmonic visible-light-driven photocatalysts through a cascade mechanism, Ceramics Intern., 43 (2017) 13447–13460.
[40] M. Pirhashemi, A. Habibi-Yangjeh, $ZnO/NiWO_4/Ag_2CrO_4$ nanocomposites with p-n-n heterojunctions: highly improved activity for degradations of water contaminants under visible light, Sep. Pur. Techn., 193 (2018) 69–80.
[41] C.M.I. Okoye, Investigation of the pressure dependence of band gaps for silver halides within a first-principles method, Solid State Comun., 129 (2004) 69–73.
[42] F. Wang, C.D. Valentin G. Pacchioni, Electronic and structural properties of WO_3: A systematic hybrid DFT study, J. Phys. Chem., 115 (2011) 8345–8353.
[43] A. Duzynska, R. Hrubiak, V. Drozd, H. Teisseyre, W. Paszkowicz, A. Reszka, The structural and optical properties of ZnO bulk and nanocrystals under high pressure, High Pres. Res., 32 (2012) 354–363.
[44] M. Pirhashemi, A. Habibi-Yangjeh, Ultrasonic-assisted preparation of plasmonic $ZnO/Ag/Ag_2WO_4$ nanocomposites with high visible-light photocatalytic performance for degradation of organic pollutants, J. Colloid Interf. Sci., 491 (2017) 216–229.
[45] Tianyong Wang, Wei Quan, Deli Jiang, Linlin Chen, Di Li, Suci Meng, Min Chen, Synthesis of redox-mediator-free direct Z-scheme AgI/WO_3 nanocomposite photocatalysts for the degradation of tetracycline with enhanced photocatalytic activity, Chem. Eng. J., 300 (2016) 280–290.
[46] Z.Y. Zhang, D.L. Jiang, C.S. Xing, L.L. Chen, M. Chen, M.Q. He, Novel AgI decorated b-Bi_2O_3 nanosheets heterostructured photocatalyst for efficient degradation of organic pollutant with enhanced performance, Dalton Trans., 44 (2015) 11582–11591.
[47] X.N. Song, C.Y. Wang, W.K. Wang, X. Zhang, N.N. Hou, H.Q. Yu, A dissolution regeneration route to synthesize blue tungsten oxide flowers and their applications in photocatalysis and gas sensing, Adv. Mater. Interf., 3 (2016) 1500417.
[48] X. Zhang, L.Z. Zhang, T.F. Xie, D.J. Wang, Low-temperature synthesis and high visible-light-induced photocatalytic activity of $BiOI/TiO_2$ heterostructures, J. Phys. Chem. C, 113 (2009) 7371–7378.
[49] D.R. Lide (ed), CRC Handbook of Chemistry and Physics, 84th Edition. CRC Press. Boca Raton, Florida, 2003; Section 10, Atomic, Molecular, and Optical Physics; Ionization Potentials of Atoms and Atomic Ions.
[50] S.G. Bratsch, J.J. Lagowski, Predicted stabilities of monatomic anions in water and liquid ammonia at 298.15 K, Polyhedron, 5 (1986) 1763–1770.
[51] W. Chaibi, R.J. Peláez, C. Blondel, C. Drag, C. Delsart, Effect of a magnetic field in photodetachment microscopy, Eur. Phys. J. D., 58 (2010) 29–37.
[52] R.C. Bilodeau, M. Scheer, H.K. Haugen, Infrared laser photodetachment of transition metal negative ions: studies on Cr^-, Mo^-, Cu^-, and Ag^-, J. Physics B, 31 (1998) 3885–3891.
[53] S. Rothe, J. Sundberg, J. Welander, K. Chrysalidis, T.D. Goodacre, V. Fedosseev, T. Kron, Laser photodetachment of radioactive $^{128}I^-$, J. Phys. G: Nucl. Part. Phys., 44 (2017) 104003 (10 pp).
[54] A.O. Lindahl, The electron affinity of tungsten, Eur. Phys. J. D, 60 (2010) 219–222.
[55] T. Wanga, W. Quan, D. Jiang, L. Chen, D. Li, S. Meng, M. Chen, Synthesis of redox-mediator-free direct Z-scheme AgI/WO_3 nanocomposite photocatalysts for the degradation of tetracycline with enhanced photocatalytic activity, Chem. Eng. J., 300 (2016) 280–290.
[56] Sh. Zhao, Y. Zhang, Y. Zhou, K. Qiu, Ch. Zhang, J. Fang, X. Sheng, Reactable polyelectrolyte-assisted preparation of flower-like Ag/AgCl/ BiOCl composite with enhanced photocatalytic activity, J. Photochem. Photobiol. A: Chem., 350 (2018) 94–102.
[57] A. Reddy, J. Choi, S. Lee, R. Ma, T-K. Kim, Green synthesis of AgI nanoparticle–functionalized reduced graphene oxide aerogels with enhanced catalytic performance and facile recycling, RSC. Adv., 5 (2015) 67394–67404.
[58] J.-G. Ibanez, M. Hemandez-Esparza, C. Doria-Serrano A. Fregoso-Infante, (2007) Environmental Chemistry Fundamentals, 1st ed. USA. Springer, pp. 129–131.
[59] A. Bonilla-Petriciol, D.-I. Mendoza-Castillo, H.-E. Reynel, (2017) Adsorption Processes for Water Treatment and Purification, Edition: 1st. Publisher: Springer International Publishing, pp. 93–95.
[60] I. Poulios, M. Kositzi, A. Kouras, Photocatalytic decomposition of triclopyr over aqueous semiconductor suspensions, J. Photochem. Photobiol. Part A: Chem., 115 (1998) 175–183.
[61] S. Senobari, A. Nezamzadeh-Ejhieh, A comprehensive study on the enhanced photocatalytic activity of, CuO-NiO nanoparticles: Designing the experiments, J. Molec. Liq., 261 (2018) 208–217.
[62] M. Pirhashemi, A. Habibi-Yangjeh, Facile fabrication of novel $ZnO/CoMoO_4$ nanocomposites: Highly efficient visible-light-responsive photocatalysts in degradations of different contaminants, J. Photochem. Photobiol. A: Chem., 363 (2018) 31–43.
[63] Z. Dong, Y. Wu, N. Thirugnanam, G. Li, Double Z-scheme $ZnO/ZnS/g\text{-}C_3N_4$ ternary structure for efficient photocatalytic H_2 production, Appl. Surf. Sci., 430 (2018) 293–300.

[64] S. Hammad, H.M. El-Bery, A. H. EL-Shazly, M.F. Elkady, Effect of WO_3 morphological structure on its photoelectrochemical properties, Int. J. Electrochem. Sci., 13 (2018) 362–372.
[65] Z. Amani-Beni, A. Nezamzadeh-Ejhieh, NiO nanoparticles modified carbon paste electrode as a novel sulfasalazine sensor, Anal. Chim. Acta, 1031 (2018) 47–59.
[66] M. Mazloum-Ardakani, A. DehghanManshadi, M. Bagherzadeh, H. Kargar, Impedimetric and potentiometric investigation of a sulfate anion-selective electrode: Experiment and simulation, Anal. Chem., 84 (2012) 2614–2621.
[67] I. Yade, M. Fall, A.A. Diagne, Electrosynthesis of poly(3-methylthiophene) films: salt effect on the electrochemical and impedance properties, J. Iran. Chem. Soc., 9 (2012) 999–1005.
[68] R. Karimi Shervedani, M. Bagherzadeh, Electrochemical impedance spectroscopy as a transduction method for electrochemical recognition of zirconium on gold electrode modified with hydroxamated self-assembled monolayer, Sensors Actuators B: Chem., 139 (2009) 657–664.
[69] H. Chang, C. Su, C.-H. Lo1, L.-Ch. Chen, T.-T. Tsung, Ch.-S. Jwo, Photodecomposition and surface adsorption of methylene blue on TiO_2 nanofluid prepared by ASNSS, Mater. Trans., 45 (2004) 3334–3337.
[70] H. Derikvandi, A. Nezamzadeh-Ejhieh, Synergistic effect of p-n heterojunction, supporting and zeolite nanoparticles in enhanced photocatalytic activity of NiO and SnO_2, J. Colloid Interf. Sci., 490 (2017) 314–327.
[71] O.S. Ksenzhek, A.M. Petrova, V. Kolodyazhny, Electrochemical properties of some redox indicators, Bioelectroch. Bioener., 4 (1977) 346–357.
[72] S. Adhikari, D. Sarka, G. Madras, Highly efficient WO_3–ZnO mixed oxides for Photocatalysis, RSC. Adv., 5 (2015) 11895–11904.
[73] H. Lin, J. Cao, B. Luo, B. Xu, S. Chen, Synthesis of novel Z-scheme AgI/Ag/AgBr composite with enhanced visible light photocatalytic activity, Catal. Commun., 21 (2012) 91–95.
[74] R. Abe, H. Takami, N. Murakami, B. Ohtani, Pristine simple oxides as visible light driven photocatalysts: highly efficient decomposition of organic compounds over platinum-loaded tungsten oxide, J. Am. Chem. Soc., 130 (2008) 7780–7781.
[75] A. Youssef, M. Al-Awadhi, M. Akl, Solid phase extraction and spectrophotometric determination of methylene blue in environmental samples using bentonite and acid activated bentonite from Egypt, J. Anal. Bioanal. Tech., 5 (2014) 179–188.
[76] G.V. Morales, E.L. Shan, R. Cornejo, E.M. Farfan Torres, Kinetic studies of the photocatalytic degradation of tartrazine, Latin Amer. Appl. Res., 42 (2012) 45–49.
[77] M. Pirhashemi, A. Habibi-Yangjeh, Visible-light photosensitization of ZnO by Bi_2MoO_6 and AgBr: Role of tandem n-n heterojunctions in efficient charge transfer and photocatalytic performances, Mater. Chem. Phys., 214 (2018) 107–119.
[78] Junxiong Lin, L. Wang, Chong Sun, Influence factors and kinetic study on photocatalytic degradation of Rhodamine B by Fe-doped TiO_2/diatomite composite, Adv. Mater. Res., 535–537 (2012) 2209–2213.
[79] R. MohammadzadehKakhki, A. Karimian, H. HasanNejad, F. Ahsani, Zinc oxide–nanoclinoptilolite as a superior catalyst for visible photooxidation of dyes and green synthesis of pyrazole derivatives, J. Inorg. Organometal. Polym. Mater., https://doi.org/10.1007/s10904-019-01100-8.

Supplementary data

Table 1
Information used for the calculation of the crystallite size of the AgI-WO_3-ZnO composite by the Scherer equation

2θ (deg)	θ (deg)	θ (rad)	FWHM	B (rad)	Cos θ (rad)	B Cos θ (rad)	Diameter (nm)	Average d (nm)
8.9814	4.4907	0.0763	0.3936	0.0162	1	0.0162	8.5677	11.4
10.968	5.484	0.0932	0.1968	8.089e-3	1	8.089e-3	17.1355	
14.5886	7.2943	0.124	0.2952	0.0121	1	0.0121	11.4237	
16.149	8.0745	0.1373	0.2952	0.0121	1	0.0121	11.4237	
19.002	9.501	0.1615	0.5904	0.0243	1	0.0243	5.7118	
21.9538	10.9769	0.1866	0.2952	0.0121	1	0.0121	11.4237	
22.4895	11.2448	0.1912	0.1968	8.089e-3	1	8.089e-3	17.1356	
23.2143	11.6072	0.1973	0.1476	6.066e-3	1	6.066e-3	22.8474	
23.8458	11.9229	0.2027	0.1968	8.089e-3	1	8.089e-3	17.1356	
25.5503	12.7752	0.2172	0.3936	0.0162	1	0.0162	8.5678	
27.7212	13.8606	0.2356	0.1476	6.066e-3	1	6.066e-3	22.8475	
28.4295	14.2148	0.2417	0.246	0.0101	1	0.0101	13.7085	
29.1871	14.5936	0.2481	0.2952	0.0121	1	0.0121	11.4238	
36.1723	18.0862	0.3075	0.5904	0.0243	1	0.0243	5.7119	
39.3548	19.6774	0.3345	0.246	0.0101	1	0.0101	13.7086	
41.8609	20.9305	0.3558	0.5904	0.0243	1	0.0243	5.7119	
46.4547	23.2274	0.3949	0.246	0.0101	1	0.0101	13.7087	
50.0728	25.0364	0.4256	0.2952	0.0121	1	0.0121	11.424	
56.7947	28.3974	0.4828	0.5904	0.0243	1	0.0243	5.712	
58.5859	29.293	0.498	0.5904	0.0243	1	0.0243	5.712	
62.4674	31.2337	0.531	0.3936	0.0162	1	0.0162	8.5681	
71.2234	35.6117	0.6054	0.3936	0.0162	0.999	0.0162	8.5682	

Table 2
Quantitative analysis of the composite based on the EDX results

Elt	Line	Int	Error	K	Kr	W%	A%	ZAF	Ox%	Pk/Bg	LConf
O	Ka	61.7	12.0453	0.1325	0.0991	24.20	67.02	0.4096	0.00	29.93	23.33
Zn	Ka	32.3	0.4231	0.3094	0.2314	23.07	15.64	1.0029	0.00	6.92	21.93
Ag	La	76.9	1.3152	0.1877	0.1404	17.05	7.00	0.8236	0.00	8.77	16.50
I	La	46.3	1.3152	0.1734	0.1297	16.19	5.65	0.8010	0.00	6.53	15.52
W	La	6.9	0.4231	0.1970	0.1474	19.49	4.70	0.7563	0.00	3.01	17.39
				1.0000	0.7480	100.00	100.00		0.00		